

Alma Mater Studiorum Università di Bologna
Archivio istituzionale della ricerca

Dynamics augmentation for high speed flying yacht hulls through PID control of foiling appendages

This is the final peer-reviewed author's accepted manuscript (postprint) of the following publication:

Published Version:

Amoroso, C.L., Liverani, A., Francia, D., Ceruti, A. (2021). Dynamics augmentation for high speed flying yacht hulls through PID control of foiling appendages. OCEAN ENGINEERING, 221, 1-13 [10.1016/j.oceaneng.2020.108115].

Availability:

This version is available at: <https://hdl.handle.net/11585/805417> since: 2021-02-24

Published:

DOI: <http://doi.org/10.1016/j.oceaneng.2020.108115>

Terms of use:

Some rights reserved. The terms and conditions for the reuse of this version of the manuscript are specified in the publishing policy. For all terms of use and more information see the publisher's website.

This item was downloaded from IRIS Università di Bologna (<https://cris.unibo.it/>).
When citing, please refer to the published version.

(Article begins on next page)

Dynamics Augmentation for High Speed Flying Yacht Hulls through PID Control of Foiling Appendages

C. L. Amoroso^{a,*}, A. Liverani^a, D. Francia^a, A. Ceruti^a

^aDepartment of Industrial Engineering, University of Bologna, v.le Risorgimento, 2, 40136 Bologna, Italy

Abstract

A numerical investigation is conducted in order to identify a PID control loop feedback scheme able to return dynamics augmentation and superior seakeeping characteristics in the application of high speed flying yacht hulls. An existing lumped parameters model based on general unsteady equations of motion is extended and implemented in combination with a regular basic ocean waves model, to conduct parametric studies and predict the overall performances of a specific engine-propelled flying yacht hull, both in calm and rough water conditions. The unsteady behaviour of six foiling/manoeuvring appendages is investigated, the hydrodynamic characteristics being based on a database generated through the use of computational fluid dynamics methods (CFD) coupled with static/dynamic-mesh schemes. Equations of motion and hydrodynamics are solved numerically by explicit time-integration method. By comparison with control open-loop conditions, the results show the effects of the use of PID controllers in such dynamic systems in terms of seakeeping performances and dynamics augmentation.

Keywords: PID control, Foiling, Flying Yacht, Lumped Parameters Model, Hydrodynamic Performances, Ocean Waves.

List of symbols

| | | | |
|--------------|--|----------------|--|
| A_w | Regular wave amplitude | p | Angular rates of X axis |
| $A_{x,y,z}$ | Maximum sectional area in the X, Y, Z axis respectively | q | Angular rates of Y axis |
| B_{cg} | Transverse CoG position | r | Angular rates of Z axis |
| B_i | Maximum i -th component breadth | T_{max} | Maximum thrust |
| $C_{b,i}$ | Block coefficient ($= \Gamma_i / L_i B_i H_i$) | t | Time variable |
| $C_{x,i}$ | Sectional area coefficient in the X axis ($= A_x / H_i B_i$) | x, y, z | Cartesian co-ordinates |
| $C_{y,i}$ | Sectional area coefficient in the Y axis ($= A_y / H_i L_i$) | α | Angle of attack with respect to water-trajectory |
| $C_{z,i}$ | Sectional area coefficient in the Z axis ($= A_z / B_i L_i$) | $\alpha_{o,i}$ | Angle of zero-lift for the i -th yacht component |
| $Cd_{x,y,z}$ | Form drag coefficient in the X, Y, Z axis respectively | β | Side-slip angle with respect to water-trajectory |
| Fn | Yacht hull Froude number ($= V_x / \sqrt{g L_{hull}}$) | Δt | Total time of dynamic evolution |
| g | Gravity acceleration | Γ_i | Water displaced volume ($= C_{b,i} L_{w,i} B_{w,i} H_{w,i}$) |
| H_{cg} | Vertical center of gravity CoG position | θ | Angular positions of Y axis |
| H_i | Maximum i -th component height | ϕ | Angular positions of X axis |
| I | Inertia matrix of the yacht | ξ_i | Hydrodynamic correction parameter |
| L_{cg} | Longitudinal CoG position | ψ | Angular positions of Z axis |
| L_i | Maximum i -th component length | μ_a | Dynamic viscosity of air |
| m | Total mass of the yacht | μ_w | Dynamic viscosity of water |
| m_i | Mass of the i -th component | ρ_a | Mass density of air |
| N | Computation steps for the 1st solution cycle | ρ_w | Mass density of water |
| n | Computation steps for the 2nd solution cycle | Ω_B | Angular position of the yacht ($= [\phi_B, \theta_B, \psi_B]$) |

*Corresponding author

Email addresses: carmeloluca.amoroso@unibo.it (C. L. Amoroso), alfredo.liverani@unibo.it (A. Liverani), d.francia@unibo.it (D. Francia), alessandro.ceruti@unibo.it (A. Ceruti)

1 INTRODUCTION

2
3
4
5 Suffices

- 6
7 A Transom/Trailing edge-fixed reference frame
8 B Hull-fixed reference frame
9 E Earth-fixed reference frame
10 i i -th component/lifting surface of the yacht system
11

12 1. Introduction

13 Modern flying yacht hulls and sailing foilers are known [28, 51, 1629, 13] for their high performances in terms of total encountered resistance, dynamic stability and immunity to waves interference phenomena. The high performances are the result of favourable cruising heights above the sea level, which lead to a considerable decrease of hull's total wet surface. Good stability to external disturbances is the result of good designing of lifting surfaces, but sometimes this could be at the expense of penalties in terms of handling qualities and/or hydrodynamic performances [17, 29]. In real sea conditions, waves and external disturbances vary along with many factors, including yacht speed, encounter direction of waves and sea state. The system of forces acting on a basic flying yacht hull during its motion could be summarized into four main components: the lift, which is composed by the sum of all the hydrodynamic forces (resulting from the relative motion) and the hydrostatic (buoyancy) forces of the lifting surfaces, the total weight of the yacht, the thrust produced by propellers or sails, and the total encountered resistance. The latter could be further decomposed into several different components being related to friction, cross-sectional area of the lifting surfaces, transverse three-dimensional effects, wakes interference phenomena and sea-water conditions [36]. When active control is used for dynamics augmentation, additional control force components are present in the equations of motion, which are those needed for the deflection of the lifting surfaces. The maximum value of the control forces and the related change rates are both constrained by limited capability of the actuators and machinery limitations, this being a primary factor that certainly affects the choice of the control method [50]. Conventional controllers such as PIDs have been widely adopted [30, 14, 24] to cope with dynamics augmentation and stabilization for ships and crafts. Although these controllers do not belong to the optimal control category [8, 48, 50, 9], they are used due to readiness in theoretical analysis and implementation, the basic concept relying only on the response of a measured system variable and not on a mathematical knowledge of the system itself [6]. However, the PID algorithm does not guarantee an intrinsic control stability, and loop tuning/gain scheduling operations are necessary when uncertain parameters or severe nonlinearities are present in the dynamic system [24].

54 To predict overall performances in terms of stability, encountered resistance, handling qualities and dynamic behaviour, now available codes and models find application over a wide range of complexity and accuracy, which extends from complete unsteady three-dimensional numerical codes [13, 20, 49, 10, 2] to quick-simple lumped parameters models [29, 24, 22, 37, 42]. In the numerical

field, for example, Chapin et al. [13] performed a numerical investigation on a two-elements wingsail for high performance multihull yachts. The study is based on a computational (CFD) evaluation of the flow around the wingsail by resolving Navier-Stokes equations. Unsteady modeling is also used to characterize the stall behaviour and give good understanding of the flow physics that may occur in such configurations. In [20], Filippas et al. developed an unsteady boundary element method which is applied to the analysis of oscillating non-lifting bodies and flapping hydrofoils operating beneath the free surface, and in the presence of incident waves. Numerical results include the lift and thrust coefficients of the system over a range of motion parameters such as reduced frequency and Strouhal number. Fu et al. [23] used the Numerical Flow Analysis (NFA) to model breaking waves around a ship, including both plunging and spilling breaking waves, the formation of spray, and the entrainment of air. NFA solves the Navier-Stokes equations utilizing a cut-cell, Cartesian-grid formulation with interface-capturing to model the unsteady flow of air and water around moving bodies. A panellized surface representation of the ship hull is required as input in terms of body geometry, and domain decomposition is used to distribute portions of the grid over a large number of processors (HPC). Although recent numerical codes [20, 27, 26] and computational methods (CFD, FVM and NFA) [13, 10, 18, 23] are able to describe complex three-dimensional hydrodynamic fields and unsteady motions, they still require large computational resources and time consuming in terms of geometry preparation, mesh-grid generation and/or computational domain distribution processes.

From the first half of the twentieth century onwards, various yacht dynamic systems have been studied through the use of simple analytical models. Fossati et al. [22] used a simple lumped parameters model with the aim to reproduce unsteady sail aerodynamics taking into account three-dimensional effects and unsteady mainsail-jib interaction. In this study, the hull of the yacht is modelled as a single point mass constrained to move on a surface governed by the equations of wave motion. In Matveev [37], a method of hydrodynamic discrete sources is applied for two-dimensional modeling of stepped planing surfaces. The water surface deformations, wetted hull lengths, and pressure distribution are also included in the formulation. Previous published works [50, 29, 24] also explored the application of classic and modern control theory to passive and active stability of both propelled and sailing foilers. In [29] for example, the classic methods of flight dynamics are applied to the passive stability of a specific modern high performance sailing foiler. The whole system is returned to a six degrees of freedom (DOF) point and the equations of motion are solved in the frequency domain. Good insight is gained by extracting the natural modes and frequencies from the linearization of the equations. In [50], the sailing performances of a twin hull (S-SWATH vehicle) in waves are investigated. In this study, a flapping foil stabilizer is proposed to enhance the seakeeping advantages of the vehicle in rough waves. A vertical plane motion control model is built and the unsteady hydrodynamic characteristics of the flapping foil stabilizer are also investigated. In [24], an adapted

4
5 water-jet propulsion based on PID control is implemented in a high
6 speed slid-ship model to obtain active control on heave/pitch modes
7 and dynamic instabilities at the high-speed ranges.

8 In contrast to the now available CFD, NFA and numerical codes,
9 simple lumped parameters models are still largely used due to their
10 simplicity and quickness, although their inaccuracy and limited range
11 of application [42, 38, 39]. Axiomatic assumptions and restric-
12 tions are intrinsic in the use of this type of models: lumped pa-
13 rameters formulation is not suitable for capturing complex three-
14 dimensional phenomena such as free water-surface deformation and
15 wakes propagation-interaction involved in a system of lifting sur-
16 faces during unsteady motion. From the point of view of active
17 control, low degrees of freedom models give poor insight into un-
18 steadiness of coupled dynamic modes and control forces [29, 50, 24],
19 leaving out also other basic aspects of interest such as minimum
20 control speed regimes and relative deviation (errors) from desired
21 states when finite-time evolutions are involved. Different extensions
22 [20, 27] are indeed necessary to take into account such aspects, lead-
23 ing thus to more rigorous and complex formulations. In view of
24 this, the main outcome of the present work is to investigate on the
25 existence of an active PID control scheme for a specific engine-
26 propelled yacht hull, which is able to return dynamics augmentation
27 and superior seakeeping characteristics through the control of six
28 foiling/manoeuvring appendages over a specified range of cruising
29 speeds (propulsion power) and sea-water conditions. In particular, it
30 is authors' goal to conduct a numerical investigation on the minimum
31 cruising speed ranges and control force gains which are necessary to
32 obtain satisfying control/hydrodynamic performances. For the sake
33 of this, the lumped parameters model presented in [5] is extended
34 to a multi lifting surface system in conjunction with a PID control
35 loop feedback scheme. In the next section, the physical and mathe-
36 matical model of the problem will be developed and particularized to
37 the test flying yacht hull. Due to lack of (ad hoc) experimental data
38 and/or measurements, numerical CFD simulations of the test yacht
39 were conducted, the results being collected and implemented in the
40 present formulation. It is shown that the present formulation is able
41 to well capture dynamics and seakeeping performances of the aug-
42 mented flying yacht system, the results of the model being in good
43 agreement with the CFD numerical measurements over the specified
44 range of cruising speeds.

45 **2. Physical model and assumptions**

46
47
48
49 In the present work an extension of the lumped parameters model
50 presented in [5] is developed and used in order to capture the main
51 dynamic effects of a PID control system on a specific high speed fly-
52 ing yacht hull (Fig. 1) for a given set of parametric quantities and
53 initial conditions. To be in line with the authors' goals, main ef-
54 fects of interest could be stability augmentation, seakeeping perfor-
55 mances and unsteady rigid body dynamics both in calm and rough-
56 water conditions. The yacht dynamic system is returned to a six de-
57 grees of freedom point (G) of weight mg , whose three linear and

angular displacement variables are unknowns of the problem. Each
foiling and manoeuvring appendage is in turn returned to a six de-
grees of freedom point (F_i) of weight $m_i g$, whose three linear and
angular displacement variables are also unknowns of the problem.
In the present paper, the rotation around the leading edge of each
foiling and manoeuvring appendage will be considered only, the re-
maining degrees of freedom being considered fixed with respect to
the $G-X_B Y_B Z_B$ frame of reference. Furthermore, yacht pitching and
rolling dynamic modes will be mostly affected by exercising con-
trolled torque around the leading edge of four J-type foils placed al-
most symmetrically with respect to the center of gravity G, whereas
two aft vertical rudders will be used for yawing modes control (Fig.
1 and Fig. 3). Each i -th component of the yacht system has a lo-
cal frame of reference $A_i-X_{Ai} Y_{Ai} Z_{Ai}$ placed at the middle point A_i
of the respective trailing edge, and is treated as a rigid ([15, 16]) lift-
ing surface of finite thickness/span entirely characterized by its over-
all dimensions L_i, B_i, H_i , hydrostatic parameters $C_{b,i}, C_{x,i}, C_{y,i}, C_{z,i}$
and hydrodynamic coefficients $Cd_{x,i}, Cd_{y,i}, Cd_{z,i}, \xi_i, \alpha_{o,i}$. Unsteady
three-dimensional phenomena such as free water-surface deforma-
tion, wakes propagation/interaction and added masses [11, 47] are
first estimated through the use of numerical CFD evaluations, then
space-time averaged and implicitly treated in the physical model by
augmentation of basic hydrodynamic coefficients. The space-time
average process leads to hydrodynamic parameters which are unique
for each component of the yacht system but constant both in space
and time. Load, lift, resistance and thrust are treated as integrated
quantities and concentrated forces acting on their respective applica-
tion point as depicted in Fig. 1.

52 **3. Mathematical formulation**

53
54 When all the components of the yacht system and the initial con-
55 ditions of the problem are defined, the present model utilizes basic
56 unsteady motion and hydrodynamic equations to predict the tempo-
57 ral evolution of all state variables and related output quantities for
58 a given thrust, load and center of gravity location. The general un-
59 steady motion equations of a rigid body in the three directions and
60 rotations are written with respect to a reference frame which is po-
sitioned on the center of gravity of the whole dynamic system and
which is stationary with respect to it. This is the G-fixed frame of
reference $G-X_B Y_B Z_B$. Where not specified, signs of moments and ro-
tations follow the right-hand rule and are assumed to be positive in
the counterclockwise direction as depicted in Fig. 1. With respect to
the $G-X_B Y_B Z_B$ reference frame, the unsteady equilibrium equations
in the three directions and rotations could be written as

$$\mathbf{T} + \mathbf{R} + \mathbf{S} + \mathbf{P} = m \left(\frac{d\mathbf{V}}{dt} + \boldsymbol{\omega}(\boldsymbol{\omega}) \cdot \mathbf{V} \right) \quad (1)$$

$$\mathbf{M} = I \cdot \frac{d\boldsymbol{\omega}}{dt} + \boldsymbol{\omega}(\boldsymbol{\omega}) \cdot I \cdot \boldsymbol{\omega} \quad (2)$$

, where

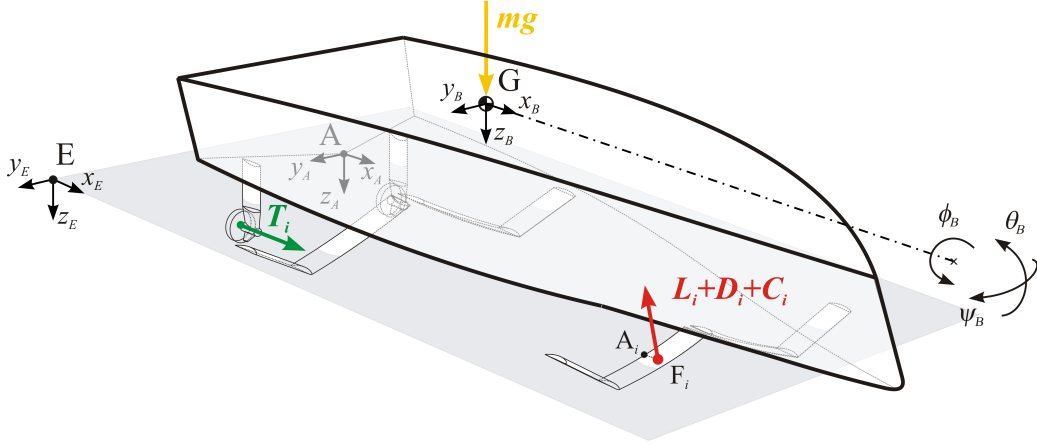


Figure 1: System of forces acting on the yacht hull.

$$\mathbf{M} = \sum_i \mathbf{x} \mathbf{T}_{B,i} \times \mathbf{T} + \sum_i \mathbf{x} \mathbf{D}_{B,i} \times \mathbf{R} + \sum_i \mathbf{x} \mathbf{B}_{B,i} \times \mathbf{S} \quad (3)$$

$$\mathbf{T} = \sum_i \mathbf{r} [\delta \phi_i, \delta \alpha_i, \delta \beta_i]^T \cdot [T_{max}, 0, 0] \quad (4)$$

$$\mathbf{P} = \mathbf{r} [\phi_B, \theta_B, \psi_B] \cdot [0, 0, mg] \quad (5)$$

$$\mathbf{S} = \sum_i \mathbf{r} [\phi_B, \theta_B, \psi_B] \cdot [0, 0, -\rho_w g \Gamma_i] \quad (6)$$

$$\mathbf{R} = \sum_i \mathbf{r} [\delta \phi_i, \delta \alpha_i, \delta \beta_i]^T \cdot [X_i, Y_i, Z_i] \quad (7)$$

$$\begin{bmatrix} X_i \\ Y_i \\ Z_i \end{bmatrix} = \begin{bmatrix} X_{f,i} \\ Y_{f,i} \\ Z_{f,i} \end{bmatrix} + \begin{bmatrix} X_{d,i} \\ Y_{d,i} \\ Z_{d,i} \end{bmatrix} + \mathbf{r} [0, \alpha_i, \beta_i] \cdot \begin{bmatrix} D_i \\ C_i \\ L_i \end{bmatrix} \quad (8)$$

$$\boldsymbol{\omega}(\omega) = \begin{bmatrix} 0 & -r_B & q_B \\ r_B & 0 & -p_B \\ -q_B & p_B & 0 \end{bmatrix} \quad (9)$$

$$\alpha_i = \arctan \left(\frac{w_i}{u_i} \right) \quad (10)$$

$$\beta_i = -\arctan \left(\frac{v_i}{u_i} \right) \quad (11)$$

and the total hydrodynamic force has been splitted into its two dynamic (\mathbf{R}) and static (\mathbf{S}) components. In the above equations, $\mathbf{V} = [V_x, V_y, V_z]$ and $\boldsymbol{\omega} = [p_B, q_B, r_B]$ are the inertial velocity vectors of the yacht system in the $G\text{-}X_B Y_B Z_B$ reference frame, whereas $[u_i, v_i, w_i]$ are the $A_i\text{-}X_{A,i} Y_{A,i} Z_{A,i}$ components of the local velocity vector relative to the atmosphere. For the i -th appendage, these components could be written as

$$\begin{bmatrix} u_i \\ v_i \\ w_i \end{bmatrix} = \mathbf{r} [\delta \phi_i, \delta \alpha_i, \delta \beta_i] \cdot (\mathbf{V} + \boldsymbol{\omega}(\omega) \cdot \mathbf{G} \mathbf{F}_i) - \mathbf{r} [\delta \phi_i, \delta \alpha_i, \delta \beta_i] \cdot (\mathbf{r} [\phi_B, \theta_B, \psi_B] \cdot \mathbf{W}_E) \quad (12)$$

where

$$\mathbf{G} \mathbf{F}_i = - \begin{bmatrix} L_{cg} \\ B_{cg} \\ H_{cg} \end{bmatrix} + \mathbf{A} \mathbf{A}_i + \mathbf{r} [\delta \phi_i, \delta \alpha_i, \delta \beta_i]^T \cdot \mathbf{A}_i \mathbf{F}_i \quad (13)$$

$$\mathbf{A} \mathbf{A}_i = [x_i, y_i, z_i]_A \quad (14)$$

and $\mathbf{A}_i \mathbf{F}_i$ is the application point of the hydrodynamic force acting on the i -th appendage. For thin and symmetrical foil sections, this application point could be assumed [1] to be nearly constant at a distance of about $0.75L_i$ from the trailing edge of the lifting surface. For thin and low-camber sections, $\mathbf{A}_i \mathbf{F}_i$ varies its position along the chord of the hydrofoil, the excursion range depending both on the relative incidence of the surface and its wetted length. This excursion will be further discussed in the next 3.3 section. In the present study, the moment equilibrium equations will be applied to the case of a flying yacht with $X_B Z_B$ as a plane of symmetry and $X_B Y_B Z_B$ as principal axes. For convenience, it is useful to write the whole system of equations in the state form by introducing an extra set of six cinematic equations in both linear and angular directions. This leads to a single set of twelve differential equations of the 1st order in the state variables $V_x, V_y, V_z, \phi_B, \theta_B, \psi_B, p_B, q_B, r_B, x_E, y_E, z_E$. This extra set of equations could be constructed through the use of the following cinematic relationships

$$\frac{d}{dt} [\phi_B, \theta_B, \psi_B] = \mathbf{R} [\phi_B, \theta_B, \psi_B] \cdot \boldsymbol{\omega} \quad (15)$$

$$\frac{d}{dt} [x_E, y_E, z_E] = \mathbf{r} [\phi_B, \theta_B, \psi_B]^T \cdot \mathbf{V} \quad (16)$$

3
4
5 which have been written in a convenient way by introducing an
6 inertial earth-fixed frame of reference $E-X_E Y_E Z_E$ and by using the
7 following rotation matrices

$$\mathbf{r}[[All, 1]] = \begin{bmatrix} \cos(\theta)\cos(\psi) \\ \sin(\phi)\sin(\theta)\cos(\psi) - \cos(\phi)\sin(\psi) \\ \cos(\phi)\sin(\theta)\cos(\psi) + \sin(\phi)\sin(\psi) \end{bmatrix} \quad (17)$$

$$\mathbf{r}[[All, 2]] = \begin{bmatrix} \cos(\theta)\sin(\psi) \\ \cos(\phi)\cos(\psi) + \sin(\phi)\sin(\theta)\sin(\psi) \\ -\sin(\phi)\cos(\psi) + \cos(\phi)\sin(\theta)\sin(\psi) \end{bmatrix} \quad (18)$$

$$\mathbf{r}[[All, 3]] = \begin{bmatrix} -\sin(\theta) \\ \cos(\theta)\sin(\phi) \\ \cos(\theta)\cos(\phi) \end{bmatrix} \quad (19)$$

$$\mathbf{R}[\phi_B, \theta_B, \psi_B] = \begin{bmatrix} 1 & \sin(\phi_B)\tan(\theta_B) & \cos(\phi_B)\tan(\theta_B) \\ 0 & \cos(\phi_B) & -\sin(\phi_B) \\ 0 & \sin(\phi_B)\sec(\theta_B) & \cos(\phi_B)\sec(\theta_B) \end{bmatrix} \quad (20)$$

8
9
10
11
12
13
14
15
16
17
18
19
20
21
22
23
24
25
26
27
28 A more extensive description about the derivation of the above equa-
29 tions could be found in [19]. The system obtained by joining Eq.
30 (1), Eq. (2), Eq. (15) and Eq. (16) has twelve unknown state vari-
31 ables which are herein evaluated numerically by an explicit time inte-
32 gration scheme based on the Runge-Kutta method for solving initial
33 value problems. The reader is referred to [34] for further informa-
34 tion about the method. Before proceeding with the integration of the
35 equations, the problem must be closed by adding explicit formulas
36 for the hydrodynamic coefficients, the water-air medium properties
37 and the PID control system.

3.1. Hydrodynamic lift

40
41 The lift acting on a lifting surface could be separated into two dis-
42 tinct components: the dynamic reaction of the fluid against the mov-
43 ing surface and the static buoyant contribution of the displaced vol-
44 ume under the free-water surface. The dynamic lift component has
45 different behaviors depending on cruising speed and/or Froud num-
46 ber range [42]: at lower speed regimes, the dynamic lift component is
47 order of magnitude smaller than the buoyant component. As speeds
48 are increased, transition or planing regime may occur [43, 42] and
49 the dynamic lift component could be the same order or greater than
50 the static one. From the classic aerodynamic theory [35] it is known
51 that for lifting surfaces of finite aspect-ratio, the lift force coefficient
52 could be expressed as a function of the relative incidence in the fol-
53 lowing form

$$c_L(\alpha_i, L_i, B_i) = \left(\frac{2\pi}{1 + 2\frac{L_i B_i}{B_i^2} \xi_i} \right) (\alpha_i - \alpha_{o,i}) \quad (21)$$

54 the related lift forces being

$$L_i = -\frac{1}{2}\rho_i(u_i^2 + v_i^2 + w_i^2)c_{z,i}L_iB_i c_L(\alpha_i, L_i, B_i) \quad (22)$$

for the Z_{Ai} -direction, and

$$C_i = +\frac{1}{2}\rho_i(u_i^2 + v_i^2 + w_i^2)c_{y,i}L_iH_i c_L(\beta_i, L_i, H_i) \quad (23)$$

for the Y_{Ai} -direction. The parametric quantity ξ_i in Eq. (21) has been introduced to take into account three-dimensional and free-water sur- face effects which are related to the real form of the i -th lifting ap- pendage [3, 32]. In this work, the value of ξ_i will be *arbitrarily* chosen and assigned to each component of the yacht system in order to obtain good agreement with the available CFD numerical data.

3.2. Hydrodynamic drag

The total encountered resistance acting on a lifting surface dur- ing its motion in water could be decomposed into several different components which are related to friction, cross-sectional area of the surface, transverse three-dimensional effects, wake profile and sea- water conditions. In this study, the total hydrodynamic drag force acting on a lifting surface is decomposed into four main compo- nents, namely, frictional, form, induced and residuary resistance. The first three components are treated explicitly through the use of semi- empirical formulas [35, 36], while the last residuary term is treated implicitly in the formulation through the use of a correction fac- tor (ξ_i) and corrected hydrodynamic coefficients ($Cd_{x,i}$, $Cd_{y,i}$, $Cd_{z,i}$). CFD simulations have been conducted and used in the present paper in order to give an estimation of the correction parameters within the speed range of interest. With respect to the local frame of reference $A_i-X_{Ai}Y_{Ai}Z_{Ai}$, the frictional, form and induced resistance components for the i -th lifting surface could be respectively evaluated through the use of the following expressions [36, 35]:

$$\begin{bmatrix} X_{f,i} \\ Y_{f,i} \\ Z_{f,i} \end{bmatrix} = \begin{bmatrix} \rho_i u_i^2 c_f(\rho_i, \mu_i, u_i, L_i) (c_{z,i}L_iB_i + c_{y,i}L_iH_i) \\ \rho_i v_i^2 c_f(\rho_i, \mu_i, v_i, B_i) (c_{z,i}L_iB_i + c_{x,i}B_iH_i) \\ \rho_i w_i^2 c_f(\rho_i, \mu_i, w_i, H_i) (c_{y,i}L_iH_i + c_{x,i}B_iH_i) \end{bmatrix} \quad (24)$$

$$\begin{bmatrix} X_{d,i} \\ Y_{d,i} \\ Z_{d,i} \end{bmatrix} = \begin{bmatrix} \frac{1}{2}\rho_i u_i^2 (c_{x,i}B_iH_i)Cd_{x,i} \\ \frac{1}{2}\rho_i v_i^2 (c_{y,i}L_iH_i)Cd_{y,i} \\ \frac{1}{2}\rho_i w_i^2 (c_{z,i}L_iB_i)Cd_{z,i} \end{bmatrix} \quad (25)$$

$$D_i = -\frac{1}{2}\rho_i(u_i^2 + v_i^2 + w_i^2)c_{z,i}L_iB_i \left(\frac{c_{z,i}L_iB_i}{\pi B_i^2} c_L^2 \right) \quad (26)$$

, where c_f is the friction coefficient calculated with the ITTC 1957 Model-Ship Correlation Line [33] and the hydrodynamic coefficients $Cd_{x,i}$, $Cd_{y,i}$, $Cd_{z,i}$ are replaced by their averaged value obtained through CFD computations within the analyzed speed range.

MATHEMATICAL FORMULATION

3.3. Center of pressure

It is shown in [42, 45] that the longitudinal position of the center of pressure of planing surfaces could be evaluated by separating the hydrodynamic lift contribute from the hydrostatic one. The center of pressure of the dynamic lift component is taken to range from 33 to 75 percent of the mean wetted length forward of the transom of conventional planing surfaces. On the other hand, the longitudinal position of the application point of the buoyancy force is found to be nearly constant at the 33 percent of the mean wetted length forward of the transom. Savitsky suggested [42] the following semi-empirical expression for the total center of pressure excursion:

$$c_{p,i} = 0.75 - \frac{1}{5.21 \left(\frac{u_i}{\sqrt{g L_{w,i}}} \right)^2 \frac{B_{w,i}}{L_{w,i}} + 2.39} \quad (27)$$

where $c_{p,i}$ is the ratio of the longitudinal distance from the transom to the center of pressure divided by the wetted length $L_{w,i}$. In the present paper, the application point of the buoyancy force component is calculated through the geometric centroid of the displaced volume ∇_i under the free-surface level, while the hydrodynamic force component is taken to range from 33 to 75 percent of the wetted length $L_{w,i}$ according to Eq. (27).

3.4. Multiphase model

The present formulation is based on a multiphase model which is used to compute the hydrodynamic forces acting on all the lifting surfaces of the analyzed yacht system. Medium properties such as mass density and dynamic viscosity are treated as integrated quantities over each lifting surface and are functions of the position of the application point where the hydrodynamic forces act.

With reference to Fig. 2 and for the i -th lifting surface of the yacht, the mass density and dynamic viscosity properties of the water-air medium could be written as

$$\begin{cases} \rho_i = \gamma_i \rho_w + (1 - \gamma_i) \rho_a \\ \mu_i = \gamma_i \mu_w + (1 - \gamma_i) \mu_a \end{cases} \quad (28)$$

where

$$\gamma_i = \frac{S_{w,i}}{c_{x,i} B_i H_i + c_{y,i} L_i H_i + c_{z,i} L_i B_i} \quad (29)$$

$$S_{w,i} = c_{x,i} S_{x,i} + c_{y,i} S_{y,i} + c_{z,i} S_{z,i} \quad (30)$$

$$\begin{bmatrix} S_{x,i} \\ S_{y,i} \\ S_{z,i} \end{bmatrix} = \begin{bmatrix} \frac{1}{2} (H d m_{w,i} + H p m_{w,i}) B_{w,i} \\ \frac{1}{2} (H d m_{w,i} + H p m_{w,i}) L_{w,i} \\ L_{w,i} B_{w,i} \end{bmatrix} \quad (31)$$

$$\begin{bmatrix} L_{w,i} \\ B_{w,i} \\ H d m_{w,i} \\ H p m_{w,i} \\ H d m_{w,i} \\ H p m_{w,i} \end{bmatrix} = \begin{bmatrix} \frac{|f(\mathbf{EA}_i) - f(\mathbf{EA}_{1,i})|}{|\sin(\theta_B + \delta\alpha_i)|} \\ \frac{|f(\mathbf{EO}_{2,i}) - f(\mathbf{EO}_{4,i})|}{|\sin(\phi_B + \delta\phi_i)|} \\ \frac{|f(\mathbf{EA}_i) - f(\mathbf{EA}_{3,i})|}{|\cos(\theta_B + \delta\alpha_i)|} \\ \frac{|f(\mathbf{EA}_{1,i}) - f(\mathbf{EA}_{2,i})|}{|\cos(\theta_B + \delta\alpha_i)|} \\ \frac{|f(\mathbf{EO}_{2,i}) - f(\mathbf{EP}_{2,i})|}{|\cos(\phi_B + \delta\phi_i)|} \\ \frac{|f(\mathbf{EO}_{4,i}) - f(\mathbf{EP}_{4,i})|}{|\cos(\theta_B + \delta\phi_i)|} \end{bmatrix} \quad (32)$$

$$\begin{bmatrix} \mathbf{EA}_i \\ \mathbf{EA}_{1,i} \\ \mathbf{EA}_{3,i} \\ \mathbf{EA}_{2,i} \\ \mathbf{EO}_{2,i} \\ \mathbf{EO}_{4,i} \\ \mathbf{EP}_{2,i} \\ \mathbf{EP}_{4,i} \end{bmatrix} = \begin{bmatrix} \mathbf{EG} - \mathbf{r}(\Omega_B)^T \cdot \mathbf{AG} + \mathbf{r}(\Omega_B)^T \cdot \mathbf{AA}_i \\ \mathbf{EA}_i + \mathbf{r}(\Omega_B + \delta_i)^T \cdot [L_i, 0, 0] \\ \mathbf{EA}_i + \mathbf{r}(\Omega_B + \delta_i)^T \cdot [0, 0, -H_i] \\ \mathbf{EA}_i + \mathbf{r}(\Omega_B + \delta_i)^T \cdot [L_i, 0, -H_i] \\ \mathbf{EA}_i + \mathbf{r}(\Omega_B + \delta_i)^T \cdot [0, 0.5B_i, 0] \\ \mathbf{EA}_i + \mathbf{r}(\Omega_B + \delta_i)^T \cdot [0, -0.5B_i, 0] \\ \mathbf{EA}_i + \mathbf{r}(\Omega_B + \delta_i)^T \cdot [0, 0.5B_i, -H_i] \\ \mathbf{EA}_i + \mathbf{r}(\Omega_B + \delta_i)^T \cdot [0, -0.5B_i, -H_i] \end{bmatrix} \quad (33)$$

$$f(\mathbf{x}) = \eta(\mathbf{x}) U(\eta(\mathbf{x})) \quad (34)$$

$$\eta(\mathbf{x}) = \mathbf{x}[[3]] - \xi(\mathbf{x}) \quad (35)$$

, $U(x)$ is the unit-step function, $\delta_i = [\delta\phi_i, \delta\alpha_i, \delta\beta_i]$ is the deflection vector of the i -th lifting surface and $\xi(\mathbf{x})$ is the wave elevation which will be discussed in the next section.

3.5. Rough-water model

This section extends the above mathematical formulation to the case of yacht motion in rough water conditions. In the present study, rough water conditions are simulated through the use of regular basic ocean waves [41] moving in the X_E -direction at the phase speed c_w . The velocity field $\mathbf{W}_E = [W_x(x, y, z), W_y(x, y, z), W_z(x, y, z)]$ associated with this type of waves could be described [41] by the following scalar components, which are written with respect to the earth-fixed reference frame $E-X_E Y_E Z_E$ and for a single wave of frequency ω_w :

$$\begin{bmatrix} W_x \\ W_y \\ W_z \end{bmatrix} = \begin{bmatrix} -\frac{A_w}{2} \omega_w \frac{\cosh\left(\frac{2\pi}{\lambda_w}(-H_w + z)\right)}{\sinh\left(-\frac{2\pi}{\lambda_w} H_w\right)} \cos\left(\frac{2\pi}{\lambda_w} x + \omega_w t\right) \\ 0 \\ -\frac{A_w}{2} \omega_w \frac{\sinh\left(\frac{2\pi}{\lambda_w}(-H_w + z)\right)}{\sinh\left(-\frac{2\pi}{\lambda_w} H_w\right)} \sin\left(\frac{2\pi}{\lambda_w} x + \omega_w t\right) \end{bmatrix} \quad (36)$$

where

$$\omega_w = \sqrt{g \frac{2\pi}{\lambda_w} \tanh\left(\frac{2\pi}{\lambda_w} H_w\right)} \quad (37)$$

is the wave frequency for a fixed ocean depth H_w . The two parameters λ_w and A_w are respectively the wavelength and the height of the

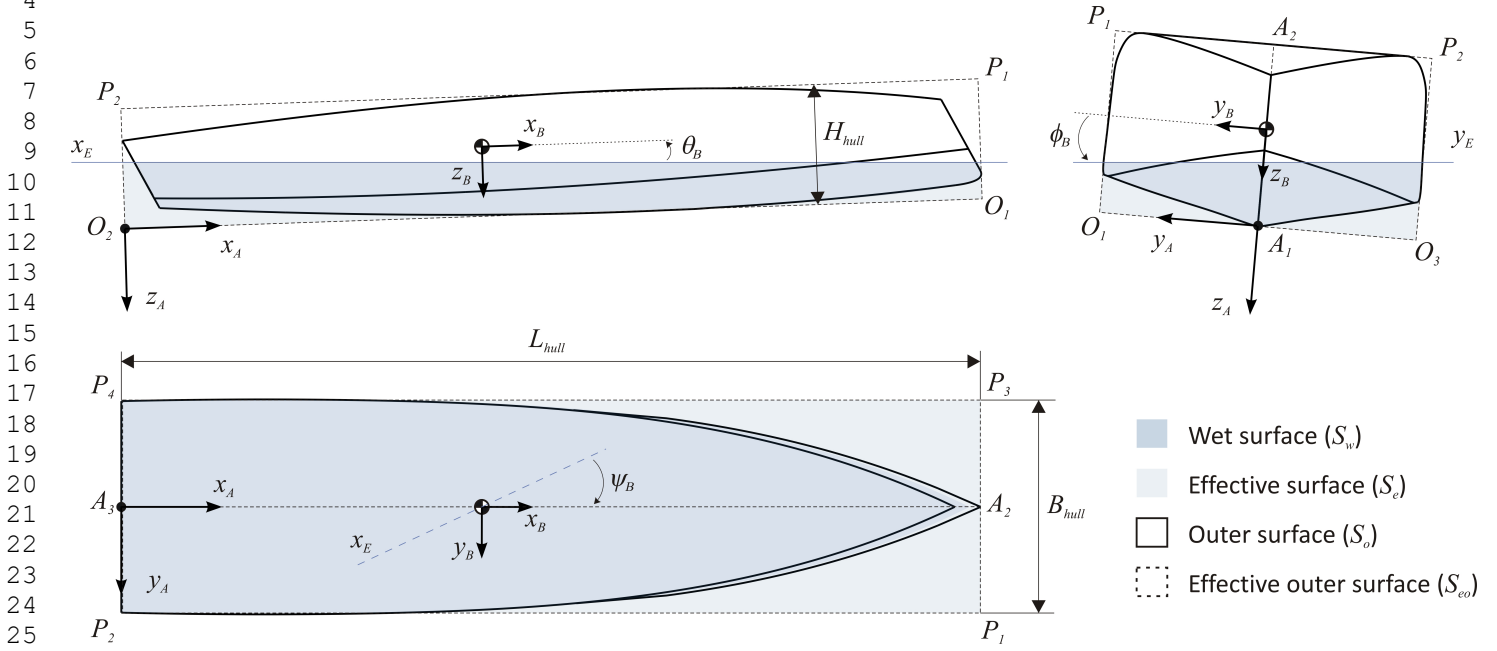


Figure 2: Multiphase model applied to each lifting surface of the yacht system. Application for the hull component only shown in figure.

30 wave. It is shown [41] that the free-water surface elevation associated
31 with the velocity field of Eq. (36) could be approximated through the
32 use of the following harmonic function

$$\xi(x) \approx \frac{A_w}{2} \omega_w \cos\left(\frac{2\pi}{\lambda_w} x + \omega_w t\right) \quad (38)$$

36 this being equivalent to considering sinusoidal wave profiles instead
37 of those obtained by direct integration of Eq. (36). Moreover, it is as-
38 sumed here that there is no slip-velocity and/or boundary layer thick-
39 ness at the water-air interface, this being considered of zero thickness
40 and placed at the wave elevation $\xi(\mathbf{x})$.

33.6. Yacht control and PID closed loop feedback scheme

44 This section of the paper presents the synthesis and the mathemat-
45 ical aspects of the PID control scheme which has been implemented
46 in the analyzed flying yacht model. In this study, a state $\mathbf{X}(t)$ will be
47 considered controlled if the relation

$$\text{Max}\left(\left|\frac{\mathbf{X}(t) - \mathbf{X}_d}{\mathbf{X}_d}\right|\right) \leq \varepsilon_o \quad (39)$$

52 is satisfied for all $t \geq \Delta t$, where ε_o is an arbitrary deviation (error)
53 from the desired state \mathbf{X}_d and Δt is the minimum time of dynamic
54 evolution which is necessary to reach steady conditions starting from
55 an initial state \mathbf{X}_o . Due to the fact that the desired states are reached
56 through the use of foiling and manoeuvring appendages, relative high
57 speed regimes are necessary to make lifting surfaces effective. In
58 particular, it is authors' interest to conduct numerical investigation
59 over a specified speed range where the relation

$$\sum_i L_i \geq mg \quad (40)$$

is satisfied for all $t \geq \Delta t$. It has to be underlined here that the total lift
force included in the present mathematical formulation could gener-
ally exceed the total weight force of the yacht. This is especially true
when either unsteady transitional regimes or motions out of symme-
try plane are involved: in both cases, the inertial terms of the r.h.s. of
Eq. (1) become explicit in Eq. (40). Equating the two sides of Eq.
(40) and substituting Eq. (22) in Eq. (40), it follows that a minimum
cruising speed of

$$V_{min} = \sqrt{\frac{mg}{\sum_i \frac{1}{2} \rho_i c_{z,i} L_i B_i c_L(\delta_{max})}} \quad (41)$$

is a necessary condition for the yacht to obtain both foiling and con-
trol, δ_{max} being the maximum allowed deflection of the appendages
before hydrodynamic stall and/or cavitation insurgence [1, 7, 13]. In
the present formulation, a saturation threshold for all the angular dis-
placement variables δ_i has been introduced when lifting surfaces are
controlled by the PID control system, maximum deflections being
limited according to the relation

$$\delta_i = F(\delta_i) \quad (42)$$

where F is a clip-function which is here defined as

$$F(\delta_i) = \delta_i U(\delta_i + \delta_{max})(1 - U(\delta_i - \delta_{max})) + \delta_{max} U(\delta_i - \delta_{max}) + \delta_{max}(1 - U(\delta_i + \delta_{max})) \quad (43)$$

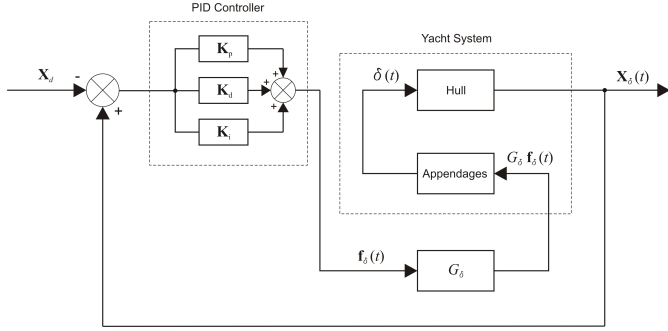


Figure 4: PID closed-loop (positive) feedback scheme used for the present yacht system.

and U is the unit-step function. This implies that the angular deflections δ_i are not allowed to exceed the value δ_{max} , whatever the amplitude of the control forces is.

As already mentioned above, before proceeding with the integration of the 6-DoF system obtained by joining Eq. (1), Eq. (2), Eq. (15) and Eq. (16), the problem must be closed by adding extra DoFs for all foiling/manoeuvring appendages and explicit formulas for PID control.

With reference to Fig. 3, the deflections $\delta\alpha_i$ of the four foiling appendages are herein used to control the pitching and rolling dynamic modes of the flying yacht, whereas the $\delta\beta_i$ deflections of the two manoeuvring appendages are used to control the dynamic yawing modes. It has to be underlined that in the analyzed flying yacht model there is no relative motion between the manoeuvring appendages and the aft propellers, the thrust vector \mathbf{T}_i being fixed to the X_{Ai} axis for i equal to $rud1$ and $rud2$. In the present paper, each foiling and manoeuvring appendage is returned to a dynamic subsystem of mass m_i , spring constant k_i and damping factor c_i , all parameters being collected in their respective diagonal matrices \mathbf{m}_δ , \mathbf{k}_δ and \mathbf{c}_δ . The angular displacement variables $\delta = [\delta\alpha_{foil1}, \delta\alpha_{foil2}, \delta\alpha_{foil3}, \delta\alpha_{foil4}, \delta\beta_{rud1}, \delta\beta_{rud2}]$ are the extra DoFs to be added in the yacht system. With respect to the i -th local reference frame $A_i-X_{Ai}Y_{Ai}Z_{Ai}$, the unsteady equilibrium equations in both Z_{Ai} (foiling) and Y_{Ai} (manoeuvring) directions could be written for all the appendages and collected as follows

$$\mathbf{m}_\delta \cdot (\mathbf{r}_\delta \cdot \ddot{\delta}) + \mathbf{c}_\delta \cdot (\mathbf{r}_\delta \cdot \dot{\delta}) + \mathbf{k}_\delta \cdot (\mathbf{r}_\delta \cdot \delta) = G_\delta \mathbf{f}_\delta + [Z_i, \dots, Y_i] \quad (44)$$

where $\mathbf{r}_\delta = [\dots, \mathbf{A}_i \mathbf{F}_i[[1]], \dots]$ is the application point of the hydrodynamic forces (Z_i, Y_i), \mathbf{f}_δ is the vector of the control forces and G_δ is a dimensionless global gain for the PID control system. For the control loop feedback scheme [6] of Fig. 4, the overall control function could be expressed in time domain as

$$\mathbf{f}_\delta = \mathbf{K}_p \cdot (\mathbf{X}_\delta - \mathbf{X}_d) + \mathbf{K}_d \cdot \dot{\mathbf{X}}_\delta - \dot{\mathbf{X}}_d + \mathbf{K}_i \cdot \int_0^t (\mathbf{X}_\delta - \mathbf{X}_d) dt \quad (45)$$

where \mathbf{X}_δ is the vector of the state variables which must be controlled

and \mathbf{X}_d is the final desired state. It has to be underlined here that the derivative action in Eq. (45) is ideal (i.e. not casual) and improves settling time and stability of the system by predicting its behaviour. Hence, an approximation of the overall PID control function might indeed be necessary. In the present paper, the following discrete form of Eq. (45) will be implemented:

$$\mathbf{f}_\delta \approx \mathbf{K}_p \cdot (\mathbf{X}_\delta - \mathbf{X}_d) + \mathbf{K}_d \cdot \frac{\Delta(\mathbf{X}_\delta - \mathbf{X}_d)}{\Delta t} + \mathbf{K}_i \cdot \Delta[\mathbf{X}_\delta - \mathbf{X}_d] \quad (46)$$

, where

$$\frac{\Delta \mathbf{X}(t)}{\Delta t} = \frac{\mathbf{X}(t) - \mathbf{X}(t - \Delta t/N)}{\Delta t/N} \quad (47)$$

$$\Delta[\mathbf{X}(t)] = \sum_{i=1}^N \left(\mathbf{X} \left(t - i \frac{\Delta t}{N} \right) \right) \frac{\Delta t}{N} \quad (48)$$

are the discrete forms of the derivative and integral operators, respectively. In Eq. (47) and Eq. (48), the quantity N is the number of iteration steps (or subdivisions) within the 1-st computation cycle, which will be discussed in the next section. Furthermore, the state variables ϕ_B , θ_B , ψ_B and z_E will be the components of the controlled state vector \mathbf{X}_δ . From a practical point of view, it has to be underlined here that while the three rotational state variables could be ready to be measured providing gyroscope sensors, the linear state variable z_E is not directly measurable and must be read (or estimated) indirectly. From a physical point of view, if the difference $\mathbf{X}_\delta - \mathbf{X}_d$ is not zero due to the fact that external disturbances are present during the motion of the yacht, control forces must deflect the foiling/manoeuvring appendages accordingly, in order to counteract the external disturbances and minimize the deviation from the desired state. Where not specified, the signs of moments and rotations follow the right-hand rule and are assumed to be positive in the counterclockwise direction as depicted in Fig. 1, Fig. 2 and Fig. 3. Hence, for the case of longitudinal stability control, if a positive trim angle error is present, a negative pitching moment must be exerted on the yacht to minimize the error, the respective deflections of the fore/aft foiling appendages being opposite in sign. The same procedure also applies to the lateral stability control, leading thus to the following structures for the PID gain matrices, which will be here used according to the arrangement of the appendages in the analyzed yacht model:

$$\mathbf{K}_p = k_p \begin{bmatrix} +a_{p,\phi} & -a_{p,\theta} & 0 & +a_{p,z} \\ -a_{p,\phi} & -a_{p,\theta} & 0 & +a_{p,z} \\ +a_{p,\phi} & +a_{p,\theta} & 0 & +a_{p,z} \\ -a_{p,\phi} & +a_{p,\theta} & 0 & +a_{p,z} \\ 0 & 0 & +a_{p,\psi} & 0 \\ 0 & 0 & +a_{p,\psi} & 0 \end{bmatrix} \quad (49)$$

NUMERICAL EVALUATIONS

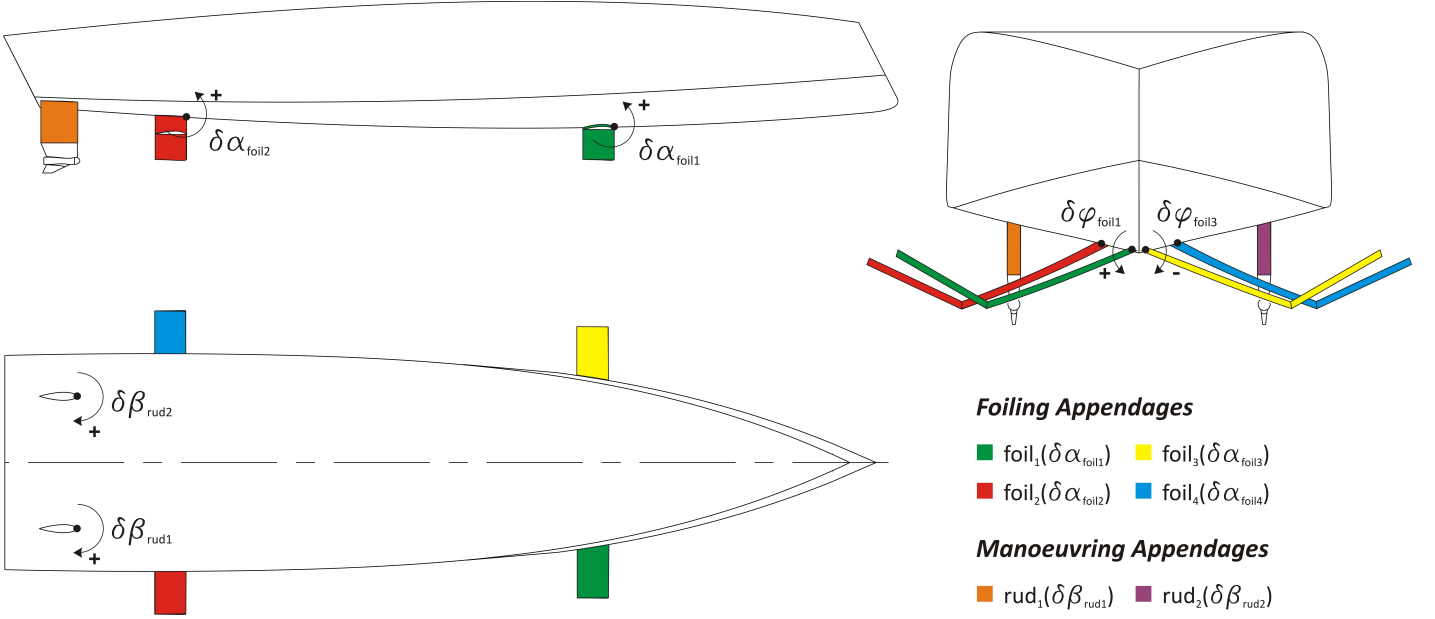


Figure 3: Reconstructed CAD model of the flying yacht. Curvatures are corrected through the approach discussed in [12]. Appendages deflections for PID control also shown in figure.

$$\mathbf{K}_d = k_d \begin{bmatrix} +a_{d,\phi} & -a_{d,\theta} & 0 & +a_{d,z} \\ -a_{d,\phi} & -a_{d,\theta} & 0 & +a_{d,z} \\ +a_{d,\phi} & +a_{d,\theta} & 0 & +a_{d,z} \\ -a_{d,\phi} & +a_{d,\theta} & 0 & +a_{d,z} \\ 0 & 0 & +a_{d,\psi} & 0 \\ 0 & 0 & +a_{d,\psi} & 0 \end{bmatrix} \quad (50)$$

$$\mathbf{K}_i = k_i \begin{bmatrix} +a_{i,\phi} & -a_{i,\theta} & 0 & +a_{i,z} \\ -a_{i,\phi} & -a_{i,\theta} & 0 & +a_{i,z} \\ +a_{i,\phi} & +a_{i,\theta} & 0 & +a_{i,z} \\ -a_{i,\phi} & +a_{i,\theta} & 0 & +a_{i,z} \\ 0 & 0 & +a_{i,\psi} & 0 \\ 0 & 0 & +a_{i,\psi} & 0 \end{bmatrix} \quad (51)$$

where $[k_p, k_d, k_i] = [2.5, 25, 0.5]$ are dimensionless quantities and

$$\begin{bmatrix} a_{p,\phi} \\ a_{p,\theta} \\ a_{p,\psi} \\ a_{p,z} \end{bmatrix} = \begin{bmatrix} 20 N/rad \\ 25 N/rad \\ 2 N/rad \\ 2 N/m \end{bmatrix} \quad (52)$$

$$\begin{bmatrix} a_{d,\phi} \\ a_{d,\theta} \\ a_{d,\psi} \\ a_{d,z} \end{bmatrix} = \begin{bmatrix} 10 N/rad/sec \\ 25 N/rad/sec \\ 2 N/rad/sec \\ 4 N/m/sec \end{bmatrix} \quad (53)$$

$$\begin{bmatrix} a_{i,\phi} \\ a_{i,\theta} \\ a_{i,\psi} \\ a_{i,z} \end{bmatrix} = \begin{bmatrix} 5 N/rad * sec \\ 12.5 N/rad * sec \\ 2 N/rad * sec \\ 5 N/m * sec \end{bmatrix} \quad (54)$$

are the respective gains of the PID matrices, the relative signs being chosen according to the above considerations. In this study, manual loop tuning operations are performed until yacht dynamic response returns satisfying control qualities within both the time interval Δt and the speed range of interest. Once the control criteria (Eq. (39)) are met, all the parameters are collected in the respective gain matrices and used in the numerical evaluations.

4. Numerical evaluations

To perform a parametric study of the foregoing unsteady equations of motion, the numerical scheme presented in [5] will be implemented in the present work. The numerical scheme is based on two computation cycles of N and n iteration steps respectively. A total evolution time Δt is chosen *a-priori*. This interval time must be large enough to ensure that the solution reaches steady state conditions. In the present study, a total evolution time of 25 seconds was found to be sufficient large to yield steady calculations at all the cruising speed values. During each step of the two cycles, the (6+4)-DoFs system obtained by joining Eq. (1), Eq. (2), Eq. (15), Eq. (16) and Eq. (44) is solved numerically by explicit time integration based on the Runge-Kutta method [34, 25, 21]. A dynamic controlled time step size is used in this method and the reader could find more specific information about the solution control and stability in [34, 25, 21].

The solution of the unsteady hydrodynamic problem is first calculated N times in the 1-st cycle. At the end of each step (i.e. when the dynamic response of the system covers the total interval of time $\Delta t/N$), input parameters are updated following a 1-st cycle scheduled table of values. The 1-st computation cycle ends as soon as the total

5 VALIDATION

evolution time Δt is fully covered. Subsequently, the same procedure applies to the 2-nd cycle with n iteration steps, input parameters being updated following a 2-nd cycle scheduled table of values. At the end of each cycle, a vector of the desired output variables is stored for post-processing operations. The solution of the problem is calculated a total of $N \times n$ times. In the present study, while the 1-st computation cycle is used for explicit time integration of the system solution, the 2-nd computation cycle is used to conduct parametric studies on the dynamic response of the system itself. An averaged number of $N = 10000$ subdivisions for the temporal evolution Δt was found to be sufficient large to reach solution convergence and capture yacht dynamics in a satisfactory manner, the 2-nd cycle iteration steps varying according to the parametric studies requirements.

5. Validation

To establish the reliability of the present mathematical model, a validation analysis is performed. Validation analysis consists of a qualitative comparison between the results obtained with the present formulation and available CFD numerical data. Numerical resistance, trim and elevation measurements at control open-loop conditions with motion in the longitudinal plane of symmetry are selected for the validation of the present results. The validation is performed for a particular test flying yacht model (Fig. 3) and within a specific cruising speed range, i.e. from 20 knts up to 50 knts. Results for variables outside the validation range are also shown and are to be considered as an extrapolation of the present formulation. Overall dimensions and parameters of each component of the yacht model are listed in Table 1 for convenience. Standard NACA series sections [1] have been used here for all the lifting surfaces, in particular NACA-4412 and NACA-0012 for foiling and manoeuvring appendages respectively. For this type of foil sections, a value of $\delta_{max} = 12^\circ$ has been chosen as a maximum allowed deflection in order to avoid non-linearities, hydrodynamic stall and/or cavitation insurgence [1, 7, 13].

Steady mean values for the hydrodynamic coefficients of each component of the test yacht are estimated using RANSE method [10, 13] with single-phase model and static-mesh scheme [49, 40]. Hydrodynamic performances of the yacht system at foiling mode with in-plane motion are estimated with both multiphase VOF model and dynamic-mesh scheme [31, 46]. In all the CFD computations, the standard $k - \varepsilon$ model [10] has been implemented for modeling the turbulence of the flow. Test conditions of present formulation are set according to the CFD numerical measurements and for the same flying yacht model. Where it is not specified, the test model is considered at rest conditions when $t = 0 \text{ sec}$, the steady output quantities being collected after a time interval of Δt . Moreover, the two aft thrust vectors are fixed in magnitude during each temporal evolution, the quantity T_{max} following a scheduled table of values according to the yacht cruising speed requirements.

The yacht system presented and analyzed in this paper showed motion instabilities [24] in pitch/heave dynamic modes for a cruising

Table 1

Geometric/hydrodynamic parameters of the test flying yacht model.

| Parameter | Component | | | | | |
|-------------------------------|-------------|---------------------------|----------------------------|---------------------------|----------------------------|---------------------------|
| | <i>hull</i> | <i>leg</i> _{1,3} | <i>foil</i> _{1,3} | <i>leg</i> _{2,4} | <i>foil</i> _{2,4} | <i>rud</i> _{1,2} |
| L_i (m) | 15.00 | 0.52 | 0.52 | 0.52 | 0.52 | 0.65 |
| B_i (m) | 4.16 | 1.49 | 1.00 | 1.80 | 1.00 | 0.08 |
| H_i (m) | 2.09 | 0.06 | 0.06 | 0.06 | 0.06 | 0.83 |
| m_i (kg) | 8500 | 125 | 125 | 125 | 125 | 250 |
| k_i (N/m) | - | 0.00 | 0.00 | 0.00 | 0.00 | 0.00 |
| c_i (N/m/s) | - | 2.5e06 | 2.5e06 | 2.5e06 | 2.5e06 | 2.5e06 |
| $x_{A,i}$ (m) | 0.00 | 9.68 | 9.68 | 2.53 | 2.53 | 0.65 |
| $y_{A,i}$ (m) | 0.00 | ± 0.74 | ± 1.89 | ± 0.86 | ± 2.15 | ± 1.20 |
| $z_{A,i}$ (m) | 0.00 | 0.30 | 0.27 | 0.18 | 0.31 | 0.49 |
| $\delta\phi_i$ ($^\circ$) | 0.00 | ± 21 | ± 32 | ± 21 | ± 27 | 0.00 |
| $\delta\alpha_i$ ($^\circ$) | 0.00 | var. | var. | var. | var. | 0.00 |
| $\delta\beta_i$ ($^\circ$) | 0.00 | 0.00 | 0.00 | 0.00 | 0.00 | var. |
| $c_{b,i}$ (-) | 0.75 | 0.65 | 0.65 | 0.65 | 0.65 | 0.65 |
| $c_{x,i}$ (-) | 0.72 | 1.00 | 1.00 | 1.00 | 1.00 | 1.00 |
| $c_{y,i}$ (-) | 0.89 | 0.64 | 0.64 | 0.64 | 0.64 | 1.00 |
| $c_{z,i}$ (-) | 0.47 | 1.00 | 1.00 | 1.00 | 1.00 | 0.64 |
| $Cd_{x,i}$ (-) | 0.75 | 0.10 | 0.10 | 0.10 | 0.10 | 0.48 |
| $Cd_{y,i}$ (-) | 1.11 | 0.86 | 0.86 | 0.86 | 0.86 | 1.15 |
| $Cd_{z,i}$ (-) | 1.23 | 1.15 | 1.15 | 1.15 | 1.15 | 0.86 |
| ξ_i (-) | 0.00 | 1.50 | 1.50 | 1.50 | 1.50 | 0.50 |
| $\alpha_{o,i}$ (-) | 0.00 | -4.00 | -4.00 | -4.00 | -4.00 | 0.00 |

speed range of $V_x \geq 35 \text{ kts}$ and for deflections of $\delta\alpha_i \geq 6^\circ$. In test conditions, all lifting surfaces are locked at their nominal incidences, which are chosen so that

$$\delta\alpha_i = \begin{cases} 0^\circ & \text{if } V_x \geq 35 \text{ kts} \\ \delta\alpha_{max} = 6^\circ & \text{otherwise} \end{cases} \quad \forall t \geq 0 \quad (55)$$

$$\delta\beta_i = \begin{cases} 0^\circ & \text{in-plane motion} \\ -2^\circ & \text{otherwise} \end{cases} \quad \forall t \geq 0 \quad (56)$$

in order to avoid the motion instabilities. It has to be underlined here that $\delta\alpha_{max}$ and δ_{max} are actually two different values of maximum allowed deflections, which are related to each other through the trim attitude of the yacht system and the hydrodynamic incidence of the lifting surfaces in the following manner:

$$\delta_{max} = \delta\alpha_{max} + (\theta_B)_{max} + (\alpha_i)_{max} \quad (57)$$

Fig. 5 shows a comparison between CFD numerical measurements and results obtained with the present model. Although its basis on lumped parameters and simplifying assumptions, the model has shown good agreement with the results, the corresponding comparison errors being between 1.5 and 33 percent for the output quantities within the specific speed range. As reported in figure, the trends in the yacht total resistance, trim and heave curves are well captured by present formulation, showing good qualitative/quantitative agreement between CFD measurements and present results. A better esti-

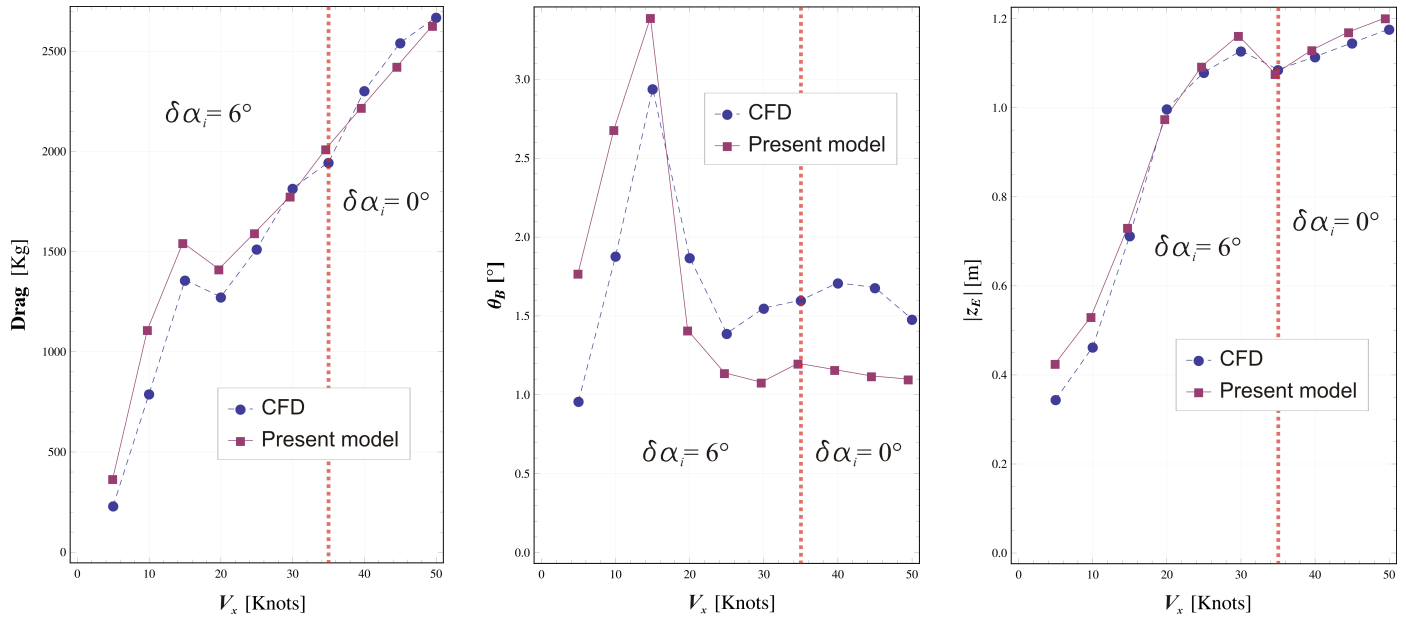


Figure 5: Comparison between present results and CFD numerical measurements.

information could be sought for the trim angle θ_B , which is the state variable most affected by three-dimensional effects such as free-water surface deformation and wakes interference phenomena. When the Froude number of the yacht hull lies below its critical value [44] of 0.4 (i.e. $V_x \approx 9$ kts), the bulk of the yacht weight is mostly supported by the hydrostatic buoyancy of the hull [4, 27]. In this low-speed regime, the hydrodynamic forces acting on all the lifting surfaces of the yacht (including the hull) are too low to return either planing or foiling conditions. For the present test yacht model it has been found, indeed, that a minimum cruising speed of $V_{min}(\delta_{max}) \approx 20$ kts (Eq. (41)) is necessary to obtain foiling conditions, which is more than twice the critical speed value of the yacht hull. This could also be verified from Fig. 5, where considerable yacht elevations z_E are reached only after $V_x \approx 20$ kts. Within the mid speed range 9 kts $< V_x < 20$ kts planing regime occurs, the yacht being still largely supported by the hydrodynamic forces acting on its hull. In this speed range, variations of the state variable z_E are also the effect of yacht rotation and trimming attitudes θ_B . Hence, for the whole speed range 0 kts $< V_x < 20$ kts the approach discussed in [5] could be more suitable to give a better approximation of the reached steady states if sought. Moreover, it has to be underlined that the parametric quantity ξ_i of Eq. (21) has been chosen ad hoc and arbitrarily for the specific flying yacht model (Table 1) used in present results. Matching with numerical measurements is strongly affected by this parameter and additional CFD and/or experimental database is needed when both shapes and dimensions of the appendages are changed or altered.

6. Results and discussion

This section of the paper presents the results which have been obtained through the use of the above formulation when the control loop feedback scheme of Fig. 4 is implemented. Results are related to the same flying yacht model of the validation test case and the CFD numerical measurements. What is expected from the present analysis is the existence of a PID algorithm capable of returning - over the specified range of cruising speed - an augmentation of yacht dynamics in terms of stabilization and state control, both in calm and rough water conditions. It is main purpose to investigate on the minimum cruising speed regimes and control forces which are necessary to obtain low deviation (errors) from the desired states \mathbf{X}_d and satisfying yacht control.

6.1. Yacht performances in calm water conditions

In the previous section, yacht performances at open-loop control mode have been evaluated and shown, all foiling/manoeuvring appendages being locked at their nominal incidence. From a physical point of view, the higher the yacht cruising elevations are, the greater the reduction of the total wet surface is. This could also result in a reduction of the total encountered resistance if no accelerations were present in the advancement direction. In this section, the PID control scheme will be used to control the yacht elevations within the speed range of interest in order to obtain a further reduction of the total wet surface with respect to the basic uncontrolled system (Fig. 5). Evaluations are performed in calm water conditions and with yacht motion in the longitudinal plane of symmetry. A desired state of $\mathbf{X}_d = [\phi_B, \theta_B, \psi_B, z_E] = [0^\circ, 0.25^\circ, 0^\circ, -1.20 \text{ m}]$ has been chosen, the choice depending on the fact that cruising elevations higher than 1.20

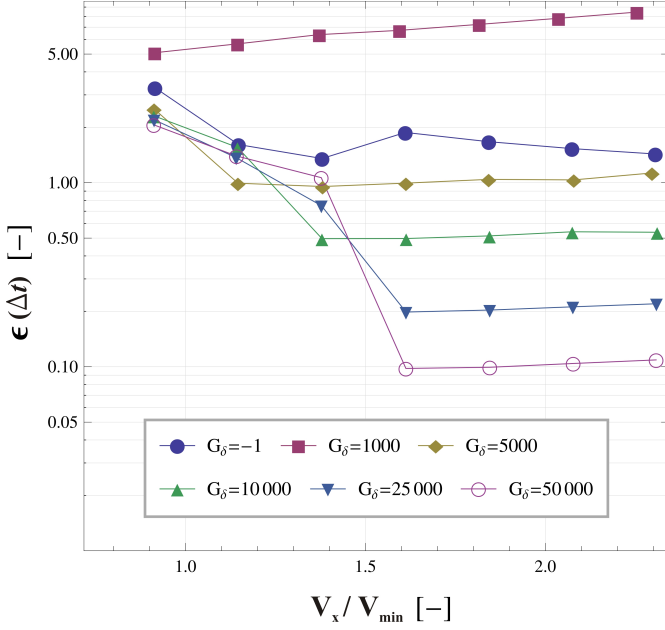


Figure 6: Maximum deviation error from the desired state \mathbf{X}_d .

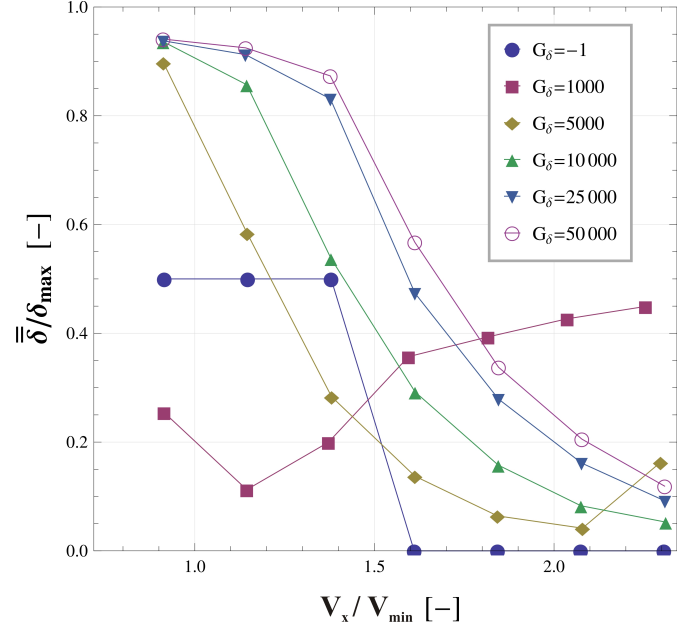


Figure 7: Mean plus standard deviation of the angular deflection vector δ .

lead foiling appendages to become (control) ineffective due to poor wet surface. Furthermore, a low trim angle of $\theta_B = 0.25^\circ$ has been chosen here as desired pitching attitude in terms of handling/comfort qualities.

As already mentioned above, the analyzed yacht system has shown a minimum cruising speed of $V_{min}(\delta_{max}) \approx 20 kts$ as a necessary condition to enter foiling mode. This value of speed is well different from the minimum *control speed* of the flying yacht, which must be a function of the desired state \mathbf{X}_d , the control gain G_δ and the allowed deviation error ϵ_o . To underline this difference, Fig. 6 shows the maximum deviation error $\epsilon(\Delta t) = \text{Max} \left(\left| \frac{\mathbf{X}_\delta(\Delta t) - \mathbf{X}_d}{\mathbf{X}_d} \right| \right)$ obtained for six different values of the control gain G_δ when the desired state is \mathbf{X}_d . A value of -1 for the gain G_δ means that open-loop conditions are treated and control system is not active, all foiling/manoeuvring appendages being locked at their respective nominal incidence (Eq. (55)).

From Fig. 6 it could be seen that for the analyzed flying yacht a control gain value greater than $5.0e+04$ is necessary to reach the desired state \mathbf{X}_d with a deviation error below 0.1. Furthermore, there is a specific cruising speed for each G_δ curve at which the maximum deviation error reaches its lower value. Above this cruising speed, the hydrodynamic forces tend to overcome the control forces and higher values of the gain are needed to not increase the deviation error. In the right half of the plot (i.e. $V_x \gtrsim 1.6V_{min}$), high values of G_δ are mostly associated with controlled states of lower deviation error, giving good control capabilities and stability augmentation in the dynamic response of the yacht system. In the low speed range, on the other hand, a value of $5.0e+03$ for the gain G_δ is necessary to maintain a deviation error below the unity, lower values resulting

in a complete loss of control for all the cruising speeds. Conversely, values which are higher than $5.0e+03$ are not necessarily associated with lower deviation error states. This is consistent with the fact that control forces must be large enough to overcome the hydrodynamic forces acting on the foiling appendages, but not too large to excessively deflect the moving surfaces. Excessive deflections could result in a large increase of total encountered resistance, this affecting yacht trim attitudes in a severe way. From this point of view, Fig. 7 and Fig. 8 show the maximum value obtained when a mean plus standard deviation operator (\equiv) is applied to each component of the angular deflection vector δ and control force vector \mathbf{f}_δ , respectively.

As it could be seen from Fig. 7, almost all G_δ curves decrease monotonically with respect to the cruising speed, this underlining the fact that lower deflections of foiling appendages are needed for control when higher hydrodynamic forces are present. The same considerations also apply to the magnitude of the control forces (Fig. 8): for a value of V_x which is well above $\approx 1.6V_{min}$, part of the energy needed to control and move the lifting surfaces could be extracted from the hydrodynamic forces themselves. This is valid until the PID control loop feedback mechanism reaches its intrinsic residual steady-state error (SSE) [6], which could be mitigated by increasing either the \mathbf{K}_i integral term in Eq. (45) or the control gain G_δ . It has to be underlined here that, although the presence of an integral action in the implemented control scheme, the existence of a residual steady-state error is possible due to the fact that a finite time Δt has been chosen for yacht dynamics evolution.

From Fig. 7 it could also be seen that there are two exceptions in the trend of the G_δ curves, i. e. when the control gain assumes the value of $5.0e+03$ and $1.0e+03$, respectively. In the first case, a

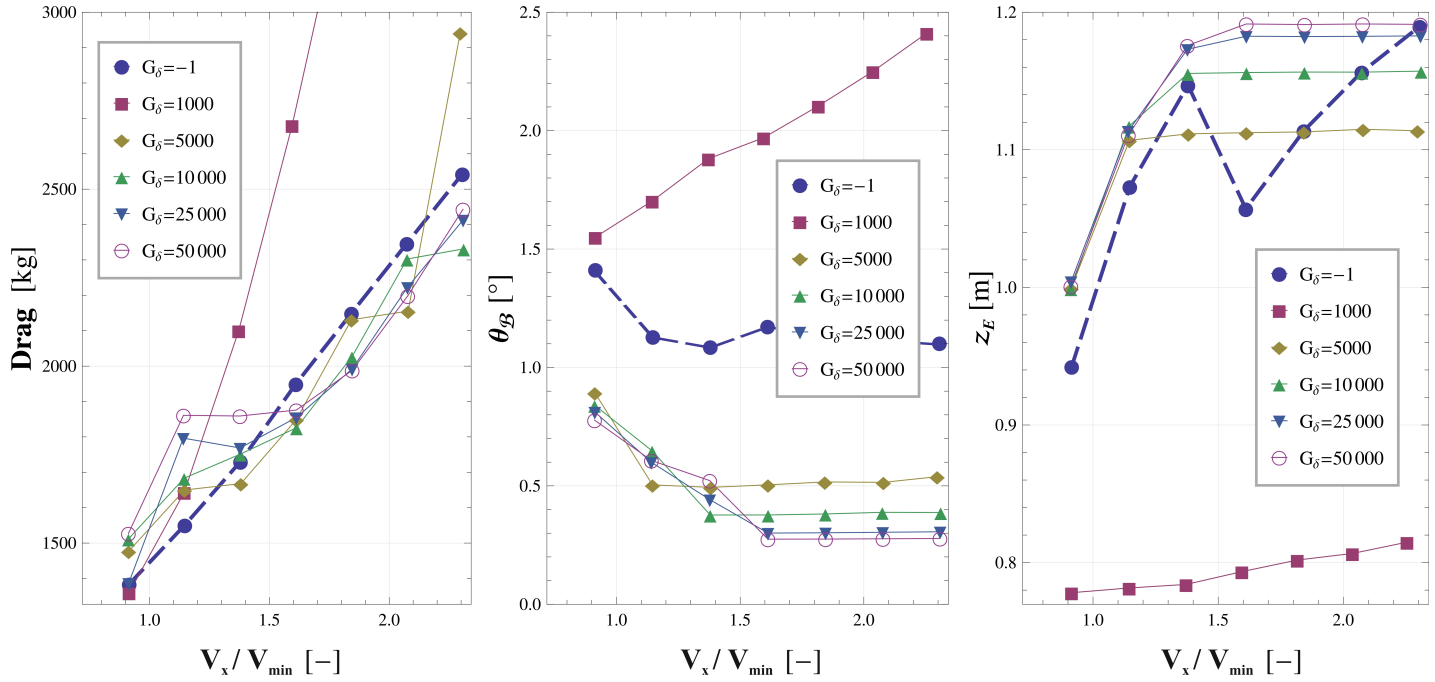


Figure 9: Yacht performances at PID control closed-loop mode for six different values of the control gain G_δ . Open-loop conditions with nominal deflections also shown in figure (blue thick dashed lines).

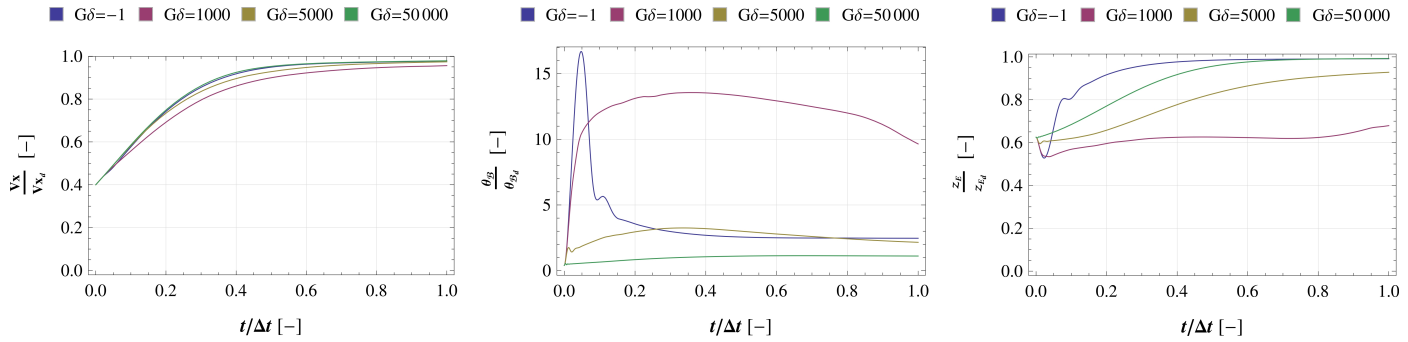


Figure 10: Temporal evolution of yacht state variables starting from $\mathbf{X}_o = [V_x, \theta_B, z_E] = [V_{min}, 0.1^\circ, -0.75 \text{ m}]$. Quantities are dimensionless with respect to \mathbf{X}_d components.

sudden increase in the lifting surface deflection is measured as soon as the ratio V_x/V_{min} exceeds the value of 2.0, this underlining the fact that the hydrodynamic forces are of the same order of magnitude of the control forces at this speed regime; in the second case, the control forces are too low to overcome the hydrodynamic forces at all the cruising speeds, this leading to a complete loss of control for the angular position vector δ , which is totally dictated by the unsteadiness of the hydrodynamic forces. An uncontrolled deflection of lifting surfaces could in turn result in a severe increase of yacht total resistance (see next Fig. 9). In this latter case, an increment of either the spring or the damping factors ($\mathbf{k}_\delta, \mathbf{c}_\delta$) in Eq. (44) could mitigate the unfavorable effect, but this is at the expense of an increase in both the magnitude and the change rate of the control forces. For the analyzed flying yacht system, it could be

seen from Fig. 8 that there is a specific cruising speed range (i.e. $1.1V_{min} \leq V_x \leq 1.6V_{min}$) where control forces reach their lowest values, the interval $5.0e+03 \leq G_\delta \leq 10.0e+03$ being a compromise between supply energy and active control characteristics. Higher values of G_δ would lead to better control and handling qualities, but the magnitude of the control forces could become very high and unfeasible from a practical point of view.

Fig. 9 shows yacht performances in terms of total encountered resistance, trim attitude and elevation when the PID controller is at closed-loop mode and for six different values of the control gain G_δ . By comparison with open-loop conditions (blue dashed lines in figure) and with regard to the output quantity of the total encountered resistance, the examined speed range could be subdivided into two distinct parts: it could be seen that active control is desirable only

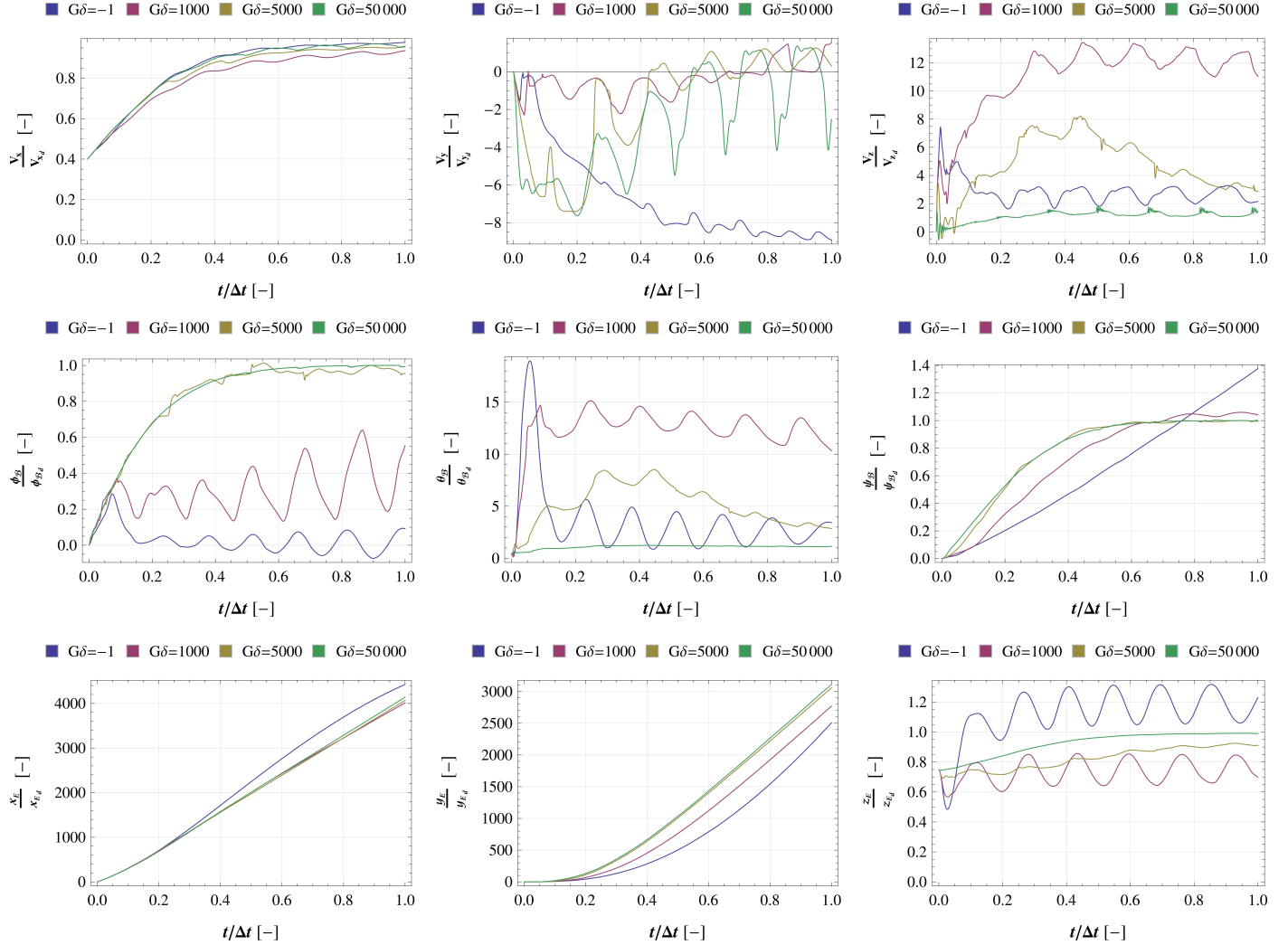


Figure 11: Temporal evolution of yacht state variables during manoeuvre in rough water conditions.

in the high speed range, its effect being not beneficial if cruising speed lies below the value of $\approx 1.6V_{min}$. In the latter case, control forces tend to establish the desired state \mathbf{X}_d overcoming the hydrodynamic forces with very high deflections of the lifting surfaces. This inevitably leads to a considerable increase in the total encountered resistance, the effect being more severe as soon as G_δ becomes large. Conversely, if control forces become too small within the range of the higher cruising speeds, hydrodynamic forces tend to overly deflect all the foiling appendages, leading to a further increase in the yacht resistance. This is the case of $G_\delta = 5.0e+03$ when cruising speeds are higher than $\approx 2V_{min}$. From Fig. 9 it could also be seen that there is a control gain value (within the range $1.0e+03 \div 5.0e+03$) below which none of the examined cruising speeds is useful for resistance reduction. In the same figure, yacht trim attitude and CoG elevation curves are also shown: as already mentioned before, high values of the control gain G_δ ($> 5.0e+03$) are necessary to reach the

desired state \mathbf{X}_d within the time interval Δt in a satisfactory manner, lower values leading to a complete loss of control at all the cruising speeds. Although a limit value of $G_\delta = 5.0e+03$ is characterized by having a relative high deviation error above the unity (Fig. 6), it could however be sufficient in terms of stability augmentation and motion damping. This could be seen more specifically in Fig. 10, where the temporal evolutions of the controlled state variables are also shown for four different values of G_δ .

6.2. Yacht performances in rough water conditions

In the previous section the performances of the test flying yacht model have been investigated for the case of motion in the longitudinal plane of symmetry and water in calm conditions. This section extends the above results to the case of motion not on yacht symmetry plane and in rough water conditions. Due to the fact that numerical investigation is conducted on yacht state variables lying

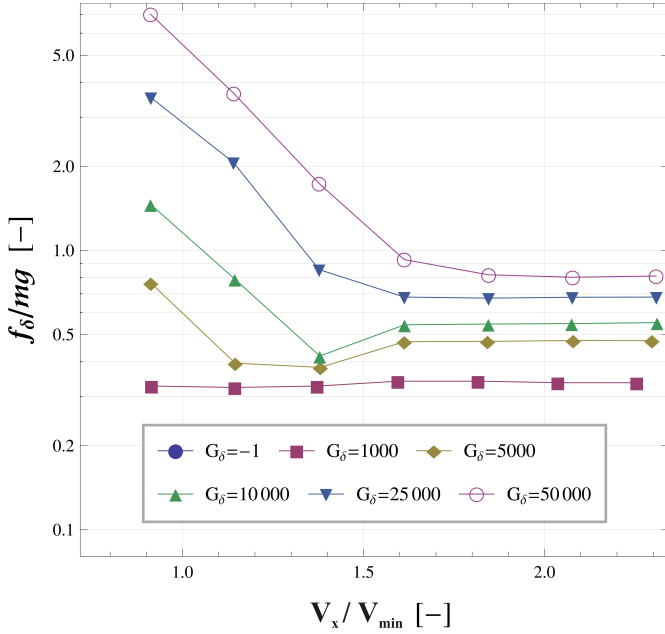


Figure 8: Mean plus standard deviation of the control forces vector \mathbf{f}_δ .

ing from an initial state vector of $\mathbf{X}_o = [V_x, \phi_B, \theta_B, \psi_B, z_E] = [V_{min}, 0^\circ, +0.1^\circ, 0^\circ, -0.75m]$. All curves in figure are shown for four different values of the control gain G_δ . By comparison with control open-loop mode ($G_\delta = -1$), it could be seen that values of G_δ higher than $5e+03$ are sufficient both to reach the desired state \mathbf{X}_d and to suppress a wave amplitude of $A_w = 25cm$ in a satisfactory manner. In particular, there are shorter transients for the yawing mode, the desired heading angle of $\psi_B = +45^\circ$ being reached more quickly than in the basic uncontrolled test case. With regard to those curves where $G_\delta = 5.0e+03$, an appreciable deviation error is still present at the end of the interval Δt , this being reducible through a further increase of either the integral term \mathbf{K}_i in Eq. (45) or the global gain G_δ , but at the expense of higher control forces. On the other hand, values of G_δ which are below $5.0e+03$ have turned out to not be beneficial in terms of yacht dynamics augmentation, all modes showing both sustained fluctuations and large deviations from the desired state \mathbf{X}_d , this being consistent with the fact that in this case surface deflections are mostly dictated by the unsteadiness of the hydrodynamic forces and not by the control system.

7. Conclusions

In the present paper, a numerical investigation has been conducted in order to identify a PID control loop feedback scheme able to return dynamics augmentation and superior seakeeping characteristics in the application of high speed flying yacht hulls. An existing lumped parameters model based on general unsteady equations of motion has been extended to a multi lifting surface system and implemented in combination with a regular basic ocean waves model, to conduct parametric studies and predict the overall performances of a specific engine-propelled flying yacht hull, both in calm and rough water conditions. The unsteady behaviour of six foiling/manoeuvring appendages has been investigated, the hydrodynamic characteristics being based on a database generated through the use of computational fluid dynamics methods (CFD) coupled with static/dynamic-mesh schemes. Equations of motion and hydrodynamics have been solved numerically by explicit time-integration method. By comparison with control open-loop conditions, the results have shown the effects of the use of PID controllers in such dynamic systems in terms of seakeeping performances and dynamics augmentation. In particular, more insight has been given on the cruising speed regimes and control force gains which are necessary to obtain satisfying control/hydrodynamic performances for the presented flying yacht model. Future areas of work include the implementation of control systems which are part of the optimal/robust control category. Future works also include parametric studies on different starting conditions and sea-water scenarios, more insight being necessary to give good understanding for a spectrum of random amplitudes and frequencies which could be involved in real sea conditions.

Acknowledgements

The authors are grateful to the University of Bologna for supporting this research study.

References

- [1] Abbott, I. H., Doenhoff, A. E. V., 1959. Theory of Wing Sections. Dover Publications Inc.
- [2] Çakici, F., Sukas, F., Usta, O., Alkan, A., 2015. A computational investigation of a planing hull in calm water by u-ranse approach. In: International Conference on Advances in Applied and Computational Mechanics.
- [3] Allroth, J., Wu, T., 2013. A cfd investigation of sailing yacht transom sterns. Master's thesis, Chalmers University of Technology, Department of Shipping and Marine Technology, Sweden.
- [4] Almeter, J., 1993. Resistance prediction of planing hulls: State of the art. Marine Technology 30 (4), 297–307.
- [5] Amoroso, C. L., Liverani, A., Caligiana, G., September 2018. Numerical investigation on optimum trim envelope curve for high performance sailing yacht hulls. Ocean Engineering 163, 76–84.
- [6] Ang, K. H., G, C., Li, Y., 2005. Pid control system analysis, design and technology. IEEE TRANSACTIONS ON CONTROL SYSTEMS TECHNOLOGY 13 (4), 559–576.
- [7] Astolfi, J. A., Bot, P., 2015. Experimental analysis of hydroelastic response of flexible hydrofoils. In: 5th High Performance Yacht Design Conference.
- [8] Athans, M., 1971. The role and use of the stochastic linear-quadratic-gaussian problem in control system design. IEEE Transactions on Automatic Control, 529–552.
- [9] Bagassi, S., Bombardi, T., Francia, D., Persiani, C., 2009. 3d trajectory optimization for uas insertion in civil non-segregated airspace. AIAA Modeling and Simulation Technologies Conference.
- [10] Bakhtiari, M., Veysi, S., Ghassemi, H., 2016. Numerical modeling of the stepped planing hull in calm water. International Journal of Engineering, Transaction B 29 (2), 236–245.
- [11] Ceruti, A., Bombardi, T., Marzocca, P., 2017. A cad environment for the fast computation of added masses. Ocean Engineering 142, 329–337.
- [12] Ceruti, A., Liverani, A., Caligiana, G., 2012. Fairing with neighbourhood lod filtering to upgrade interactively b-spline into class-a curve. International Journal on Interactive Design and Manufacturing (IJIDeM) 8, 67–75.
- [13] Chapin, V., Gourdain, N., Verdin, N., Fiumara, A., Senter, J., 2015. Aerodynamic study of a two-elements wingsail for high performance multihull yachts. In: 5th High Performance Yacht Design Conference.
- [14] Chen, Z., Gui, H., Dong, P., Yu, C., 2019. Numerical and experimental analysis of hydroelastic responses of a high-speed trimaran in oblique irregular waves. International Journal of Naval Architecture and Ocean Engineering, 409–421.
- [15] Croccolo, D., Agostinis, M. D., Fini, S., Liverani, A., Marinelli, N., Nisini, E., Olmi, G., 2015. Mechanical characteristics of two environmentally friendly resins reinforced with flax fibers. Journal of Mechanical Engineering 61 (4), 227–236.
- [16] Degidi, M., Caligiana, G., Francia, D., Liverani, A., Olmi, G., Tornabene, F., 2016. Strain gauge analysis of implant-supported, screw-retained metal frameworks: Comparison between different manufacturing technologies. Journal of Engineering in Medicine 230, 840–846.
- [17] Deng, R., bo Huang, D., li Zhou, G., 2014. Research on the influence of t-foil on the hydrodynamic performance of trimaran. In: Proceedings of the Twenty-fourth (2014) International Ocean and Polar Engineering Conference.
- [18] Duman, S., Sener, B., Bal, S., 2017. Performance prediction of a planing vessel using dynamic overset grid method. In: 11st Symposium on High Speed Marine Vehicles. Naples, Italy.
- [19] Etkin, B., 1972. Dynamics of Atmospheric Flight. John Wiley, Inc.
- [20] Filippas, E., Belibassakis, K., 2013. Free surface effects on hydrodynamic analysis of flapping foil thrusters in waves. In: Proceedings of the ASME 2013 32nd International Conference on Ocean, Offshore and Arctic Engineering.
- [21] Forsythe, G. E., Malcolm, M. A., Moler, C. B., 1977. Computer Methods for Mathematical Computations. Englewood Cliffs, NJ: Prentice-Hall.
- [22] Fossati, F., Muggiasca, S., 2012. Motions of a sailing yacht in large waves: an opening simple instationary modelling approach. In: 22th International Symposium on "Yacht Design and Yacht Construction". pp. 1–31.
- [23] Fu, T., 2012. A detailed assessment of numerical flow analysis (nfa) to predict the hydrodynamics of a deep-v planing hull. 29th Symposium on Naval Hydrodynamics Gothenburg, Sweden, 26–31.
- [24] Gao, S., dan Zhu, Q., Li, L., Wu, X., 2007. A new method of reducing slid-ship s dolphin movement phenomenon. In: Proceedings of the 2007 IEEE International Conference on Mechatronics and Automation.

- [25] Gear, C. W., 1971. Numerical Initial Value Problems in Ordinary Differential Equations. Englewood Cliffs, NJ: Prentice-Hall.
- [26] Ghassemi, H., Ghiasi, M., 2008. A combined method for the hydrodynamic characteristics of planing craft. *Ocean Engineering* 35 (35), 310–322.
- [27] Ghassemi, H., Kohansal, A., 2010. A numerical modeling of hydrodynamic characteristics of various planing hull forms. *Ocean Engineering* 37 (37), 498–510.
- [28] Grogono, J., Alexander, A., Nigg, D., 1972. *Hydrofoil Sailing*. London: Juanita Kalerghi.
- [29] Heppel, P., 2015. Flight dynamics of sailing foilers. In: *Proceedings in HPYD5*.
- [30] Hickey, N., Johnson, M., Katebi, M., Grimble, M., 1999. Pid controller optimisation for fin roll stabilisation. In: *Proceedings of the 1999 IEEE International Conference on Control Applications*. Vol. 2. pp. 1785–1790.
- [31] Hirt, C., Nichols, B., 1981. Volume of fluid (vof) method for the dynamics of free boundaries. *Journal of Computational Physics* 39 (1), 201–225.
- [32] Huetz, L., Alessandrini, B., 2011. Systematic study of hydrodynamic forces on sailing yacht hulls using parametric design and cfd state of the art. In: *30th International Conference on Offshore Mechanics and Arctic Engineering*.
- [33] ITTC, 2011. Recommended procedures and guidelines: Resistance test 7.5-02-02-01. In: *International Towing Tank Conference*.
- [34] Izzo, G., 2017. Highly stable implicit-explicit runge-kutta methods. *Applied Numerical Mathematics* 113, 71–92.
- [35] Kats, J., Plotkin, A., 1991. *Low-Speed Aerodynamics*. McGraw-Hill.
- [36] Kleijweg, N., 2016. A bare hull upright trimmed resistance prediction for high performance sailing yachts. Master's thesis, Delft University of Technology, Delft, Netherlands.
- [37] Matveev, K. I., 2012. Two-dimensional modeling of stepped planing hulls with open and pressurized air cavities. *International Journal of Naval Architecture and Ocean Engineering* 4, 162–171.
- [38] Piancastelli, L., Frizziero, L., Donnici, G., 2014. The common-rail fuel injection technique in turbocharged di-diesel-engines for aircraft applications. *Journal of Engineering and Applied Sciences* 9 (12), 2493–2499.
- [39] Piancastelli, L., Frizziero, L., Donnici, G., 2015. Turbomatching of small aircraft diesel common rail engines derived from the automotive field. *Journal of Engineering and Applied Sciences* 10 (1), 172–178.
- [40] Piancastelli, L., Gatti, A., Frizziero, L., Ragazzi, L., Cremonini, M., 2015. Cfd analysis of the zimmerman's v173 stol aircraft. *Journal of Engineering and Applied Sciences*.
- [41] Salmon, R., 2015. *Introduction to ocean waves*. Textbook, institution of Oceanography, University of California, San Diego.
- [42] Savitsky, D., 1964. Hydrodynamic design of planing hulls. *Marine Technology* 1257 (1), 71–95.
- [43] Savitsky, D., 2014. Semi-displacement hulls—a misnomer? Fourth SNAME Chesapeake Powerboat Symposium.
- [44] Savitsky, D., Gore, J., 1979. A re-evaluation of the planing hull form. *American Institute of Aeronautics and Astronautics Conference*.
- [45] Savitsky, D., Ward, N., 1954. Wetted area and center of pressure of planing surfaces at very low speed coefficients. Stevens Institute of Technology, Davidson Laboratory Report (493).
- [46] Sieber, R., Schäfer, M., 2001. Dynamic mesh schemes for fluid-structure interaction. In: *International Conference on Large-Scale Scientific Computing*.
- [47] Tueri, M., Ceruti, A., Marzocca, P., 2014. Added masses computation for unconventional airships and aerostats through geometric shape evaluation and meshing. *International Journal of Aeronautical and Space Sciences* 15 (3), 241–257.
- [48] van Amerongen, J., van der Klugt, P., van Nauta Lemke, H., 1990. Rudder roll stabilization for ships. *Automatica* 26 (4), 679–690.
- [49] Wackers, J., Deng, G., Guilmineau, E., Leroyer, A., Queutey, P., Visonneau, M., Palmieri, A., Liverani, A., 2017. Can adaptive grid refinement produce grid-independent solutions for incompressible flows? *Journal of Computational Physics* 344, 364–380.
- [50] Wang, H. D., Qian, P., Liang, X. F., Yi, H., 2016. Vertical plane motion control of an s-swath vehicle with flapping foil stabilisers sailing in waves. *Ocean Engineering*.
- [51] Welaya, Y. M. A., Abdulmotaleb, S. M., 2017. Numerical modeling of the hydrodynamic performance of hydrofoils for auxiliary propulsion of ships in regular head-waves. In: *Proceedings of the ASME 2017 36th International Conference on Ocean, Offshore and Arctic Engineering*.